arXiv:1602.07748v2 [hep-ph] 14 Mar 2016

DSiD: a Delphes Detector for ILC Physics Studies

Talk presented at the International Workshop on Future Linear Colliders (LCWS15), Whistler, Canada, 2-6 November 2015

C.T. Potter

University of Oregon

March 16, 2016

Abstract

We describe DSiD, a fast simulation Delphes detector for the International Linear Collider (ILC) based on the full simulation performance of the SiD detector. SiD is one of two detectors described in the ILC Technical Design Report (TDR). The tracking efficiency, tracking momentum resolution, electromagnetic and hadronic calorimeter energy resolution, particle identification and flavor tagging efficiencies are taken from the Detailed Baseline Design (DBD) study as described in ILC TDR Volume 4: Detectors. In a cross-check study with 4×10^6 $e^+e^- \to b\bar{b}$ events generated at $\sqrt{s} = 500$ GeV and simulated by Delphes with the DSiD detector card, these performance characteristics are measured and found to be commensurate with the DBD results. For a new physics use case example, we describe a study of Next-to-Minimal Supersymmetric $e^+e^- \to 2\chi_3 \to 2\chi_1 2h_1$ with $h_1 \to 2a_1$ or $h_1 \to b\bar{b}$ at the $\sqrt{s} = 500$ GeV ILC. The card is available on HepForge.

1 Introduction

With the discovery of the Standard Model Higgs boson at the Large Hadron Collider (LHC) [1, 2], the scientific case for the International Linear Collider (ILC) is now well established [3, 4, 5]. But the LHC has only just begun to explore the energy reach of the ILC, where the shortcomings of the SM tell us there must be new physics.

The machinery for full detector simulation of ILC events is well established [6, 7], and some fast simulation machinery is in place [8]. If, as expected, the LHC experiments announce discovery of new physics in Run 2, the need for rapid ILC phenomenology studies to evaluate the capability of the ILC for measuring the new physics will be evident. In this brief report we describe a Delphes [9, 10, 11, 12] fast detector simulation card modeled on the full simulation SiD detector performance as described in the ILC Technical Design Report (TDR) Volume 4: Detectors [13].

SiD is designed to provide excellent momentum and energy resolution over the broad range of particle energies expected at the ILC. It features a 5T solenoidal magnetic field, a vertex detector instrumented with silicon pixels for vertex reconstruction and a main tracker instrumented with silicon strips for measuring charged particle momentum. The electromagnetic calorimeter uses silicon strips in the active layers and tungsten in the passive layers for measuring electromagnetic energy deposits. The hadronic calorimeter employs glass resistive plate chambers in the active layers and steel in the passive layers for measuring hadronic energy deposits. The muon system is instrumented with scintillators in the iron flux return. Full details of the SiD design can be found in [13].

Delphes, a multipurpose fast detector simulator which can read StdHep [14], LHEF [15] and HepMC [16] event formats, has been used extensively for LHC pp phenomenology studies. But nothing in its architecture prevents it from use in an ILC e^+e^- environment. The current Delphes distribution now includes a detector card for the ILC Large Detector (ILD), the other ILC detector presented in the ILC TDR. We describe here the DSiD card available on HepForge [17] at `dsid.hepforge.org`.

Parameter	Value
ParticlePropagator	
Radius	2.493m
HalfLength	3.018m
Bz	5.0 T
TrackingEfficiency	
ChargedHadronTrackingEfficiency	see DBD Figure 3.5
ElectronTrackingEfficiency	see DBD Figure 3.5
MuonTrackingEfficiency	see DBD Figure 3.5
MomentumSmearing	
ChargedHadronMomentumSmearing	see DBD Figure 3.9
MuonMomentumSmearing	see DBD Figure 3.9
ElectronEnergySmearing	see DBD Figure 3.9
ECal,HCal	
ECal ResolutionFormula	$\sigma_E/E = 0.010 \oplus 0.170/\sqrt{E}$
HCal ResolutionFormula	$\sigma_E/E = 0.094 \oplus 0.559/\sqrt{E}$
Photon,Electron,Muon Efficiency	
PhotonEfficiency	see DBD Figure 10.6
ElectronEfficiency	see DBD Figure 10.7
MuonEfficiency	see DBD Figure 10.8
FastJetFinder	
JetAlgorithm	6 [antik_t]
ParameterR	1.0
InputArray	EFlowMerger/eflow
BTagging	
EfficiencyFormula 0	0.007
EfficiencyFormula 4	0.03
EfficiencyFormula 5	0.7
TauTagging	
EfficiencyFormula 0	0.001
EfficiencyFormula 15	0.4

Table 1: Delphes modules and their parameter values in DSiD. The Figures refer to the DBD figures used to specify the DSiD performance, which are reproduced in the Figures of this report for comparison to the performance measured in this study.

2 Performance Specification

Delphes simulates detector response using efficiencies and resolutions parameterized by a particle's transverse momentum and pseudorapidity or, equivalently, polar angle with respect to the beam axis. The modules which simulate the tracking response to electrons, muons and charged hadrons, in order of execution, are below.

- ParticlePropagator propagates all stable particles through the specified magnetic field
- TrackingEfficiency either kills the particle or not based on the parameterized efficiencies
- MomentumSmearing smears the particle momentum according to the parameterized resolution
- TrackMerger merges electron, muon and charged hadron tracks

For the Delphes calorimetery, either a single generic calorimeter can be specified for both electromagnetic and hadronic calorimetry or, as for DSiD, two separate calorimeters can be specified. For the latter case, the modules, in order of execution, are below.

- TrackMerger supplies track information to the calorimetry
- ECal separates eflowTracks from eflowPhotons and applies energy smearing
- HCal separates eflowTracks from eflowNeutralHadrons and applies energy smearing
- EFlowMerger merges eflowTracks with eflowNeutralHadrons and eflowPhotons

The EFlowMerger is used in case the jetfinding uses energy flow objects rather than calorimeter towers, as is the case for SiD and ILD [18]. Energy (or particle) flow algorithms associate tracks to calorimeter deposits to capitalize on superior track momentum resolution, thus giving the best possible jet energy resolution. Six possible jetfinding algorithms can be specified in the FastJetFinder module; for DSiD it is the antik_t algorithm.

Particle identification efficiencies are specified in the ElectronEfficiency, PhotonEfficiency, MuonEfficiency, BTagging and TauTagging modules. Relative or absolute isolation can be specified in the ElectronIsolation, PhotonIsolation and MuonIsolation modules.

Part II of [13], the SiD Detailed Baseline Design (DBD), contains enough information to completely specify a Delphes card. See Table 1 for the parameters used for the DSiD card. The tracking efficiencies for muons, electrons and charged pions are taken from Figure 3.5 of the DBD, the momentum smearing for tracks is taken from Figure 3.9, and the particle identification efficiencies for photons, electrons and muons are taken from Figures 10.6, 10.7 and 10.8. The electromagnetic and hadronic calorimeter energy resolution are taken to be

$$\frac{\sigma_E^{ecal}}{E} = 0.010 \oplus \frac{0.170}{\sqrt{E}} \quad (1)$$

$$\frac{\sigma_E^{hcal}}{E} = 0.094 \oplus \frac{0.559}{\sqrt{E}} \quad (2)$$

as they are in the DBD Section 4.2.2 and Figure 4.15, respectively. Calorimeter tower segmentation is defined, but the nominal DSiD card uses energy flow objects rather than towers.

In the nominal DSiD card, isolation of electrons, photons and muons is not required at the detector level since isolation can be imposed after after simulation at the analysis level. It should be noted that care should be taken with the isolation since requiring it can have an enormous impact on the performance of particle identification. If isolation is not required, the jetfinding performance can be degraded. We recommend using isolation only if the primary focus of the simulation is jetfinding and not particle identification. The nominal DSiD card uses the anti k_t algorithm with $\Delta R = 1.0$.

For the b-tag, the nominal DSiD card assumes 70% efficiency for b-jets, 3% efficiency for c-jets, and 0.7% efficiency for light jets. These values are taken from two points in Figure 10.9 of the DBD. Other b-tag operating points from that Figure can also be specified. For the τ-tag, no performance is given in the DBD, so a conservative 40% efficiency for τ-jets with 0.1% for all others are specified.

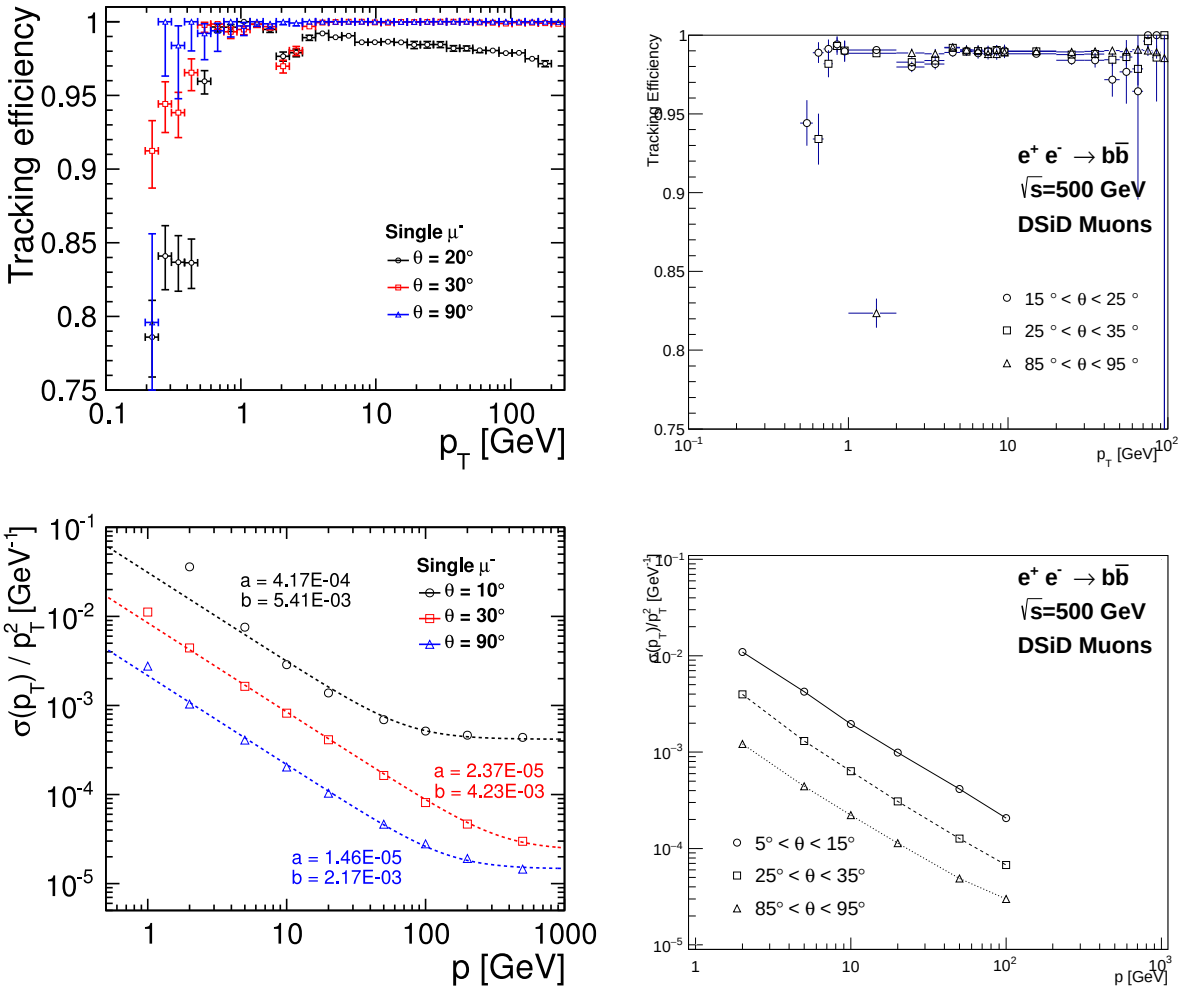

Figure 1: Tracking efficiency (top) and resolution (bottom). At left, DBD Figures 3.5 (top) and 3.9 (bottom). At right, results of this study.

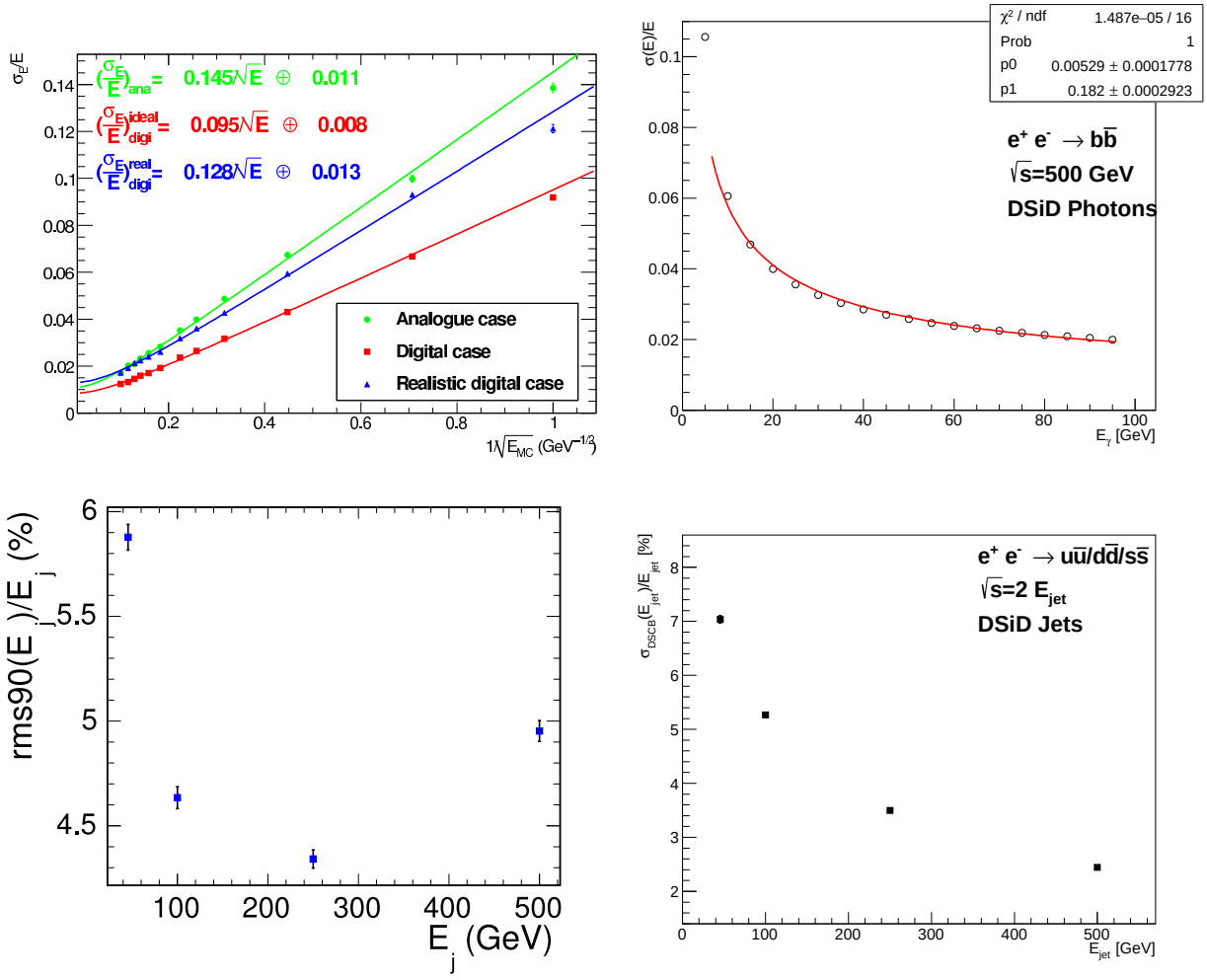

Figure 2: Photon energy resolution (top) and jet energy resolution (bottom). At left, DBD Figures 4.6 (top) and 10.11 (bottom). At right, results of this study. The photon energy resolution fit is to a model $\sigma_E^{ecal}/E = p_0 \oplus p_1/\sqrt{E}$ with free parameters p_0 and p_1. Figure 4.6 shows the expected performance of the MAPS calorimeter option, not the nominal SiD electromagnetic calorimeter, and is shown here only for comparison.

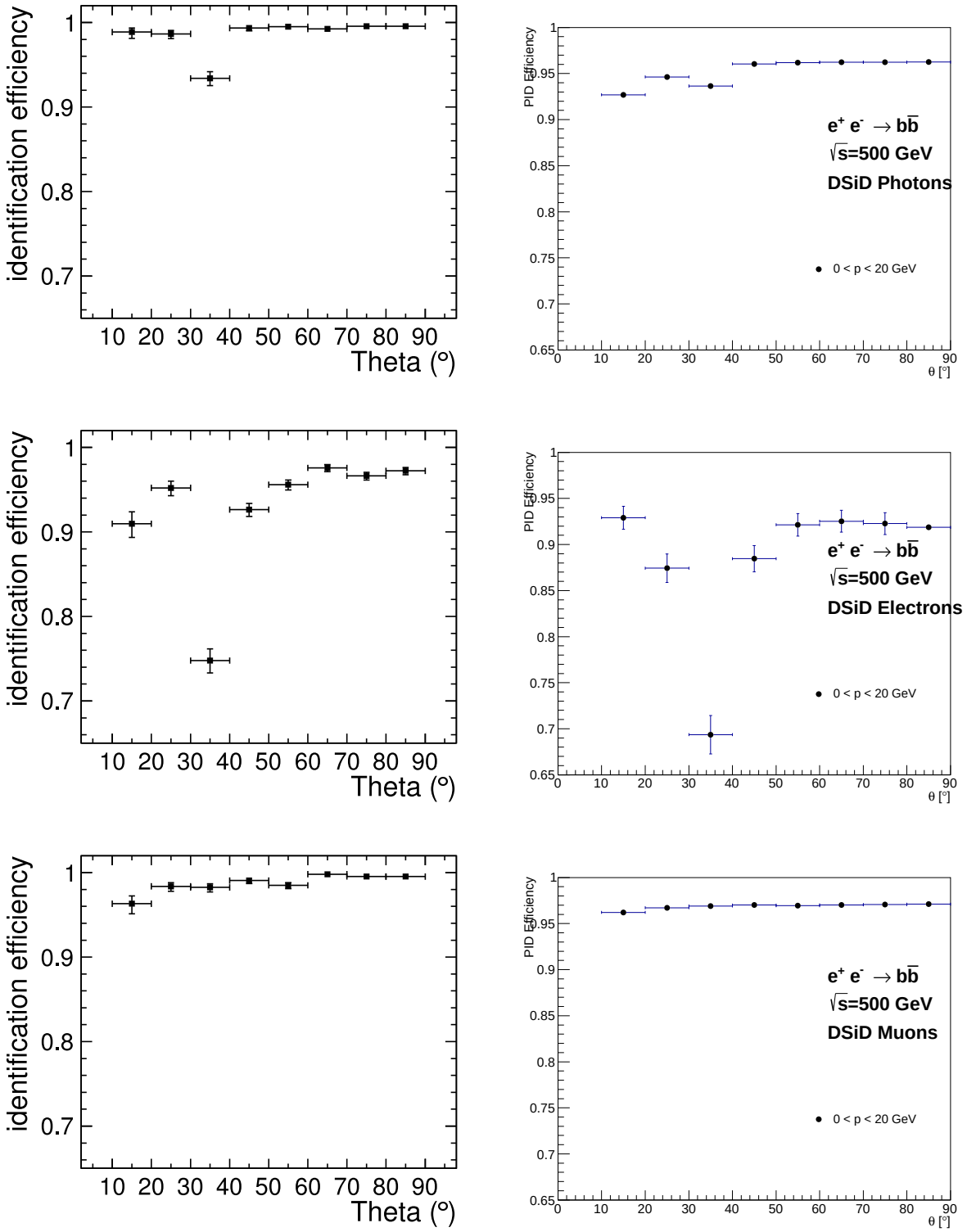

Figure 3: Particle identification efficiency for photons (top), electrons (middle) and muons (bottom). At left are Figures 10.6, 10.7 and 10.8 of the DBD, which consider objects with momentum $p = 10$ GeV objects. At right are the results of this study, which consider objects with momentum $0 < p < 20$ GeV.

3 Performance Validation

The SiD DBD performance characteristics documented in [13] were typically measured with monoenergetic or fixed-angle particles. In order to ensure that these performance characteristics can be recovered using fast simulation in a challenging event environment with many particles and a wide spectrum of energy and momentum, we generate 4×10^6 events with MG5_aMCv2.3.3 [19], specifying $e^+e^- \to b\bar{b}$ at $\sqrt{s} = 500$ GeV and StdHep output format. In order to measure the b-tag mistag rates for charm and light jets, we have also generated 10^6 $e^+e^- \to c\bar{c}$ events and 10^6 $e^+e^- \to u\bar{u}, d\bar{d}, s\bar{s}$ events. In order to study jet energy resolution, we have generated 10^6 light dijet events $e^+e^- \to u\bar{u}/d\bar{d}/s\bar{s}$ events at $\sqrt{s} = 91, 200, 500, 1000$ GeV. We then use Delphes3.3.1 for detector simulation on these events.

For tracking efficiency and momentum resolution from the DBD and as measured in this study, see Figure 1. The DBD studies use single muons with fixed polar angle $\theta = 10^\circ, 20^\circ, 30^\circ, 90^\circ$. In this study we take muons in a range within 5° of these choices for θ. The performance in the complex $e^+e^- \to b\bar{b}$ event environment matches the DBD performance well, with any differences likely due to continuous θ ranges or underpopulated phase space.

For photon and jet energy resolution, see Figure 2. No isolation is imposed for the photon energy resolution analysis, but isolation for electrons and photons is required for the jet energy resolution analysis. Fitting the photon energy resolution distribution to $\sigma_E^{ecal}/E = p_0 \oplus p_1/\sqrt{E}$ yields values close to, though not identical to the DBD values. The small differences are likely attributable to the low E_γ and high E_γ regions, which are overpopulated in the low and underpopulated in the high. For the jet energy resolution analysis, jets are reconstructed with the antik_T algorithm with $\Delta R = 1.0$ using isolated energy flow objects. The isolation requires a maximum of 12% (25%) relative E_T (p_T) in a cone of radius $\Delta R = 0.5$ around electrons and photons (muons). For non-isolated objects, the jet energy resolution performance is reduced. For this study, the energy resolution is taken from the width of the core Gaussian in a double sided Crystal Ball (DSCB) fit, while for the DBD study it is taken to be the RMS of the smallest interval containing 90% of jets. For $E_{jet} = 45, 100$ GeV, the energy resolution with Delphes is about 1% worse than for the DBD jet energy resolution while it is better for $E_{jet} = 250, 500$ GeV. The jet energy resolution at low energy is understood since no optimization for DSiD over isolation, jet algorithm, or jet parameters has been made in this study. At high jet energy, Delphes does not account for energy leakage while the full simulation DBD result does.

For electron, photon and muon particle identification efficiency, see Figure 3. Generator muons are considered identified if the reconstructed muon points to a parent generator muon with the identical energy to the true muon energy. For the electron and photon particle identification analysis, we first reject generator electrons which lose energy to bremsstrahlung and photons which convert. For photons, conversions are first vetoed by considering only generator photons with no electrons reconstructed in a radius of $\Delta R = 0.3$ around the photon. To be considered identified, a photon must be reconstructed within $\Delta R = 0.3$ of the generator photon and satisfy a loose requirement on the reconstructed photon energy, requiring it to be within 5σ of the true energy. Similarly electrons losing energy to bremsstrahlung are vetoed by considering only generator electrons with no reconstructed photons in a radius of $\Delta R = 0.3$ around the electron. To be considered identified, the electron must be reconstructed within $\Delta R = 0.3$ of the generator electron and satisfy a loose requirement on the reconstructed electron energy, requiring it to be within 5σ of the true energy.

For the c- and uds-jet mistagging rates for the four efficiency operating points considered (60%, 70% 80% and 90%), see Figure 4. We evaluate the flavor tagging performance with DSiD by measuring the efficiency to identify reconstructed b-, c- and uds-jets for the nominal DSiD tagging performance as well as three other operating points described by 60%, 80% and 90% b-tag efficiency. Events with ISR or FSR are rejected by requiring exactly two reconstructed jets.

4 Physics Example

To illustrate a new physics use case for DSiD, we describe a brief study of neutralino pair production at the $\sqrt{s} = 500$ GeV ILC. Backgrounds are not evaluated, so the signal selection is not optimized.

The Next-to-Minimal Supersymmetric Standard Model (NMSSM) is an attractive version of Supersymmetry [20] which solves the μ-term problem of the Minimal Supersymmetric Standard Model (MSSM) by introducing a Higgs singlet in addition to the two Higgs doublets of the MSSM [21, 22]. The NMSSM phenomenology includes seven Higgs bosons $a_1, a_2, h_1, h_2, h_3, H^+, H^-$, five neutralinos $\chi_1, \chi_2, \chi_3, \chi_4, \chi_5$ and four charginos $\chi_1^+, \chi_1^-, \chi_2^+, \chi_2^-$. For references to other phenomenological studies of NMSSM neutralino pair production at linear colliders, see [21].

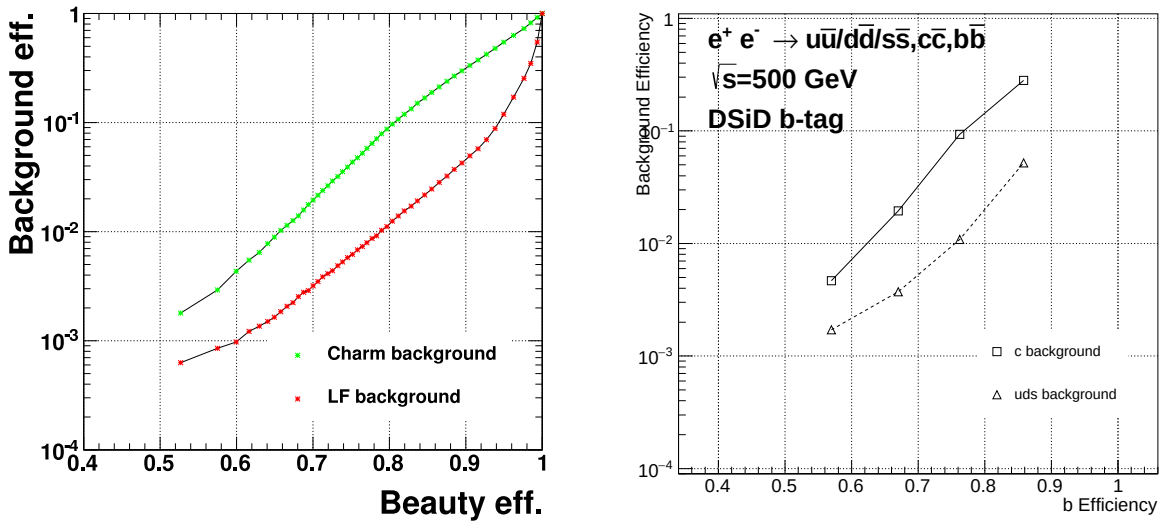

Figure 4: Efficiencies for c- and uds-jet versus the b-jet efficiency. At left is the DBD Figure 10.9, at right is the result of this study. The b-tag efficiencies in DSiD are set to 60/0.4/0.1%, 70/2/0.3%, 80/10/1% and 90/30/5% for $b/c/uds$, respectively.

We assume the NMSSM benchmark point h_{60} described in [23]. In h_{60}, pair production of all five neutralinos and all four charginos is accessible at the $\sqrt{s} = 500$ GeV ILC. Moreover, through neutralino cascade decays lighter Higgs bosons a_1 and h_1 are accessible. The 125 GeV Higgs boson discovered at the Large Hadron Collider (LHC) [1, 2] is identified in h_{60} as the dominantly doublet h_2, while the lighter h_1 and a_1 are dominantly singlet. In h_{60} the singlet is largely decoupled from the doublets, allowing the singlet to avoid exclusion by LHC searches which typically assume MSSM signatures. The lightest Supersymmetric particle (LSP) in h_{60} is the singlino χ_1.

In h_{60}, $m_{a_1} \approx 10$ GeV, $m_{h_1} \approx 56$ GeV and $m_{\chi_1} \approx 58$ GeV. The dominant decay of the χ_3 is $\chi_3 \to h_1\chi_1$. The dominant decay of the singlet dominated h_1 is $h_1 \to 2a_1$, while a subdominant decay is $h_1 \to b\bar{b}$. Since the cross section for $e^+e^- \to \chi_3\chi_3$ is of order 200 pb at the $\sqrt{s} = 500$ GeV, this makes $e^+e^- \to \chi_3\chi_3 \to 2h_1 2\chi_1 \to 4a_1 2\chi_1$ a promising channel for precision measurement of the singlet Higgs sector of the NMSSM. The dominant a_1 decay is $a_1 \to \tau^+\tau^-$, but the clean channel $a_1 \to \mu^+\mu^-$ is still accessible with a branching ratio near 0.3%.

We assume the running scenario G-20 described in [24], namely $\int dt\mathcal{L} = 5000$ fb^{-1}, 80% of which is split evenly between the two e^+e^- polarization configurations $P(e^-) = +80\%, P(e^+) = -30\%$ and $P(e^-) = -80\%, P(e^+) = +30\%$. For cross section and event generation, we use MG5_aMC@NLO [19], which features polarized beams and a complete NMSSM model that allows h_{60} spectrum and decay specification with SLHA [25, 26]. For detector simulation we use Delphes3.3.1 [9] with the DSiD card.

The signal selection for the $a_1 \to \mu^+\mu^-$ channel simply requires two oppositely charged muons with $p_t > 20$ GeV which satisfy $\Delta R(\mu^+, \mu^-) < 0.14$. Muon isolation in DSiD is modified to use a smaller cone size $\Delta R = 0.1$ so that the highly collimated muons from $a_1 \to \mu^+\mu^-$ do not fail the isolation requirement. For the $h_1 \to b\bar{b}$ signal selection, exactly three or exactly four jets are required, of which exactly two are required to be b-tagged. The two b jets are required to satisfy $\Delta R(b, b) < \frac{\pi}{2}$. Finally, electrons and muons are vetoed to reduce the impact of semileptonic b and c decays to neutrinos on the h_1 mass reconstruction.

For the reconstructed a_1 and h_1, see Figure 5. The non-Gaussian structure evident in the $h_1 \to b\bar{b}$ distribution is due to unmeasured neutrino energy in semileptonic meson decays. Such energy can be partially recovered with track vertexing and the p_T-corrected mass. A flat 5% jet energy scale correction has been applied.

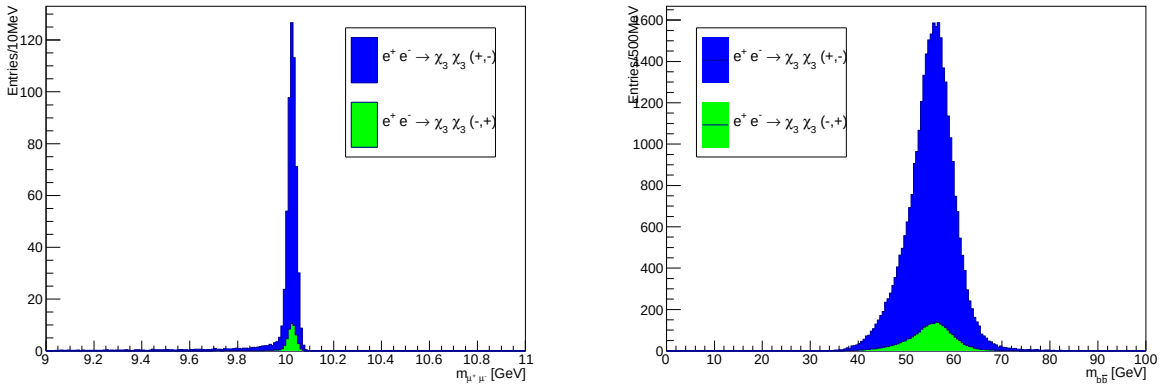

Figure 5: Reconstructed $a_1 \to \mu^+\mu^-$ (left) and $h_1 \to b\bar{b}$ (right) in $e^+e^- \to \chi_3\chi_3$ events at $\sqrt{s} = 500$ GeV. We assume 2000fb^{-1} integrated luminosity for each beam polarization configuration $P(e^+) = +80\%, P(e^-) = -30\%$ (dark) and $P(e^+) = -80\%, P(e^-) = +30\%$ (light). The signal selection has not been optimized. The non-Gaussian structure in $h_1 \to b\bar{b}$ is due to unmeasured energy from neutrinos in semileptonic meson decays.

5 Conclusion

We have described DSiD, a fast simulation Delphes detector modeled on the SiD detector. The DSiD card parameterizes the SiD full simulation performance results documented in the ILC TDR. We then carry out validation studies to confirm that the card can reproduce the SiD performance in a complex event environment $e^+e^- \to b\bar{b}$ at $\sqrt{s} = 500$ GeV. We conclude that, with some caveats, DSiD performance is consistent with the full simulation SiD DBD study.

We recommend Delphes for ILC phenomenology studies. As an example use case, we reconstruct $\chi_3 \to \chi_1 h_1$ in pair neutralino production at the $\sqrt{s} = 500$ GeV ILC with $h_1 \to b\bar{b}$ and $h_1 \to 2a_1$ with at least one $a_1 \to \mu^+\mu^-$. Evaluation and tuning of the DSiD card will be ongoing at `dsid.hepforge.org`, and we invite feedback.

Acknowledgements

The author thanks the SiD detector community for encouraging feedback and the Alder Institute for High Energy Physics for financial support.

References

[1] Georges Aad et al. Observation of a new particle in the search for the Standard Model Higgs boson with the ATLAS detector at the LHC. *Phys.Lett.*, B716:1–29, 2012, 1207.7214.

[2] Serguei Chatrchyan et al. Observation of a new boson at a mass of 125 GeV with the CMS experiment at the LHC. *Phys.Lett.*, B716:30–61, 2012, 1207.7235.

[3] Howard Baer, Tim Barklow, Keisuke Fujii, Yuanning Gao, Andre Hoang, Shinya Kanemura, Jenny List, Heather E. Logan, Andrei Nomerotski, Maxim Perelstein, et al. The International Linear Collider Technical Design Report - Volume 2: Physics. 2013, 1306.6352.

[4] Sally Dawson et al. Working Group Report: Higgs Boson. In *Community Summer Study 2013: Snowmass on the Mississippi (CSS2013) Minneapolis, MN, USA, July 29-August 6, 2013*, 2013, 1310.8361.

[5] D. M. Asner et al. ILC Higgs White Paper. In *Community Summer Study 2013: Snowmass on the Mississippi (CSS2013) Minneapolis, MN, USA, July 29-August 6, 2013*, 2013, 1310.0763.

[6] N. Graf and J. McCormick. Simulator for the linear collider (SLIC): A tool for ILC detector simulations. *AIP Conf. Proc.*, 867:503–512, 2006. [,503(2006)].

[7] M Frank, F Gaede, C Grefe, and P Mato. Dd4hep: A detector description toolkit for high energy physics experiments. *Journal of Physics: Conference Series*, 513(2):022010, 2014.

[8] Mikael Berggren. SGV 3.0 - a fast detector simulation. In *International Workshop on Future Linear Colliders (LCWS11) Granada, Spain, September 26-30, 2011*, 2012, 1203.0217.

[9] J. de Favereau, C. Delaere, P. Demin, A. Giammanco, V. Lematre, A. Mertens, and M. Selvaggi. DELPHES 3, A modular framework for fast simulation of a generic collider experiment. *JHEP*, 02:057, 2014, 1307.6346.

[10] Michele Selvaggi. DELPHES 3: A modular framework for fast-simulation of generic collider experiments. *J. Phys. Conf. Ser.*, 523:012033, 2014.

[11] Alexandre Mertens. New features in Delphes 3. *J. Phys. Conf. Ser.*, 608(1):012045, 2015.

[12] Matteo Cacciari, Gavin P. Salam, and Gregory Soyez. FastJet User Manual. *Eur. Phys. J.*, C72:1896, 2012, 1111.6097.

[13] Halina Abramowicz et al. The International Linear Collider Technical Design Report - Volume 4: Detectors. 2013, 1306.6329.

[14] L. Garren. StdHep 5.06.01 Monte Carlo Standardization at FNAL Fortran and C Implementation. `http://cd-docdb.fnal.gov/0009/000903/015/stdhep_50601_manual.ps`. Accessed: March 14, 2016.

[15] Johan Alwall et al. A Standard format for Les Houches event files. *Comput. Phys. Commun.*, 176:300–304, 2007, hep-ph/0609017.

[16] Matt Dobbs and Jorgen Beck Hansen. The HepMC C++ Monte Carlo event record for High Energy Physics. *Comput. Phys. Commun.*, 134:41–46, 2001.

[17] A. Buckley, M. R. Whalley, W. J. Stirling, J. M. Butterworth, E. Nurse, and B. Waugh. HepForge: A Lightweight development environment for HEP software. In *15th International Conference on Computing in High Energy and Nuclear Physics (CHEP 2006) Mumbai, Maharashtra, India, February 13-17, 2006*, 2006, hep-ph/0605046.

[18] M.A. Thomson. Particle flow calorimetry and the pandorapfa algorithm. *Nuclear Instruments and Methods in Physics Research Section A: Accelerators, Spectrometers, Detectors and Associated Equipment*, 611(1):25 – 40, 2009.

[19] J. Alwall, R. Frederix, S. Frixione, V. Hirschi, F. Maltoni, O. Mattelaer, H. S. Shao, T. Stelzer, P. Torrielli, and M. Zaro. The automated computation of tree-level and next-to-leading order differential cross sections, and their matching to parton shower simulations. *JHEP*, 07:079, 2014, 1405.0301.

[20] Stephen P. Martin. A Supersymmetry primer. 1997, hep-ph/9709356.

[21] Ulrich Ellwanger, Cyril Hugonie, and Ana M. Teixeira. The Next-to-Minimal Supersymmetric Standard Model. *Phys.Rept.*, 496:1–77, 2010, 0910.1785.

[22] M. Maniatis. The Next-to-Minimal Supersymmetric extension of the Standard Model reviewed. *Int.J.Mod.Phys.*, A25:3505–3602, 2010, 0906.0777.

[23] Potter, C. T. Natural NMSSM with a light Singlet Higgs and Singlino LSP. *Eur. Phys. J. C*, 76(1):44, 2016.

[24] T. Barklow, J. Brau, K. Fujii, J. Gao, J. List, N. Walker, and K. Yokoya. ILC Operating Scenarios. 2015, 1506.07830.

[25] Peter Z. Skands et al. SUSY Les Houches accord: Interfacing SUSY spectrum calculators, decay packages, and event generators. *JHEP*, 07:036, 2004, hep-ph/0311123.

[26] B. C. Allanach et al. SUSY Les Houches Accord 2. *Comput. Phys. Commun.*, 180:8–25, 2009, 0801.0045.